

# Eddy Length Scale Response to Static Stability Change in an Idealized Dry Atmosphere: A Linear Response Function Approach

Pak Wah Chan<sup>1</sup>, Pedram Hassanzadeh<sup>2</sup>, and Zhiming Kuang<sup>1</sup>

<sup>1</sup>Harvard University

<sup>2</sup>Rice University

November 24, 2022

## Abstract

The response of mid-latitude equilibrated eddies' length scale to static stability has long been questioned but not investigated in well-controlled experiments with unchanged mean zonal wind and meridional temperature gradient. With iterative use of the linear response function of an idealized dry atmosphere, we obtain a time-invariant and zonally-uniform forcing to decrease the near-surface temperature by over 2 K while keeping the change in zonal wind negligible (within 0.2 m/s). In such experiments of increased static stability, energy-containing zonal scale decreases by 3-4%, which matches with Rhines scale decrease near the jet core. Changes in Rossby radius (+2%), maximum baroclinic growth scale (-1%) and Kuo scale (0%) fail to match this change in zonal scale. These findings and well-controlled experiments help with better understanding of eddy-mean flow interactions and hence the mid-latitude circulation and its response to climate change.

1 **Eddy Length Scale Response to Static Stability Change**  
2 **in an Idealized Dry Atmosphere: A Linear Response**  
3 **Function Approach**

4 **Pak Wah Chan<sup>1\*</sup>, Pedram Hassanzadeh<sup>2,3</sup>, and Zhiming Kuang<sup>1,4</sup>**

5 <sup>1</sup>Department of Earth and Planetary Sciences, Harvard University, Cambridge, MA, USA

6 <sup>2</sup>Department of Mechanical Engineering, Rice University, Houston, TX, USA

7 <sup>3</sup>Department of Earth, Environmental and Planetary Sciences, Rice University, Houston, TX, USA

8 <sup>4</sup>John A. Paulson School of Engineering and Applied Sciences, Harvard University, Cambridge, MA, USA

9 **Key Points:**

- 10 • We use a linear response function to change static stability without changing merid-  
11 ional temperature gradient or zonal wind
- 12 • Energy-containing zonal scale decreases with increased static stability and Rossby  
13 radius
- 14 • The relative decrease in energy-containing zonal scale matches the decreased Rhines  
15 scale near the jet core

---

\*Current affiliation: College of Engineering, Mathematics and Physical Sciences, University of Exeter,  
Exeter, UK

Corresponding author: Pak Wah Chan, [pchan@eng.harvard.edu](mailto:pchan@eng.harvard.edu)

**Abstract**

The response of mid-latitude equilibrated eddies' length scale to static stability has long been questioned but not investigated in well-controlled experiments with unchanged mean zonal wind and meridional temperature gradient. With iterative use of the linear response function of an idealized dry atmosphere, we obtain a time-invariant and zonally-uniform forcing to decrease the near-surface temperature by over 2 K while keeping the change in zonal wind negligible (within  $0.2 \text{ m s}^{-1}$ ). In such experiments of increased static stability, energy-containing zonal scale decreases by 3–4%, which matches with Rhines scale decrease near the jet core. Changes in Rossby radius (+2%), maximum baroclinic growth scale (-1%) and Kuo scale (0%) fail to match this change in zonal scale. These findings and well-controlled experiments help with better understanding of eddy–mean flow interactions and hence the mid-latitude circulation and its response to climate change.

**Plain Language Summary**

In the mid-latitude atmosphere, the mean state changes the eddies, and the eddies changes the mean state. These complicated “eddy–mean flow interactions” are challenging to understand. Eddies' size is the size of the prevalent weather systems we observe, and we want to understand how it changes with increased static stability of the mean state. In simulating an increased static stability, eddies are at the same time acting to change the north-south temperature gradient of the mean state. As a result, it is difficult to attribute the eddies' response solely to the increased static stability. We manage to increase static stability without changing north-south temperature gradient in a numerical simulation, by applying a time-invariant and zonally-uniform forcing calculated from a tool called “linear response function”. As the forcing is constant with time and longitude, it can change the mean state without directly acting on eddies. Our well-controlled simulation shows that eddies' size decreases with increased static stability. This decrease matches quantitatively with a scaling argument involving non-linear processes, but do not support linear scaling arguments involving instability of vertical wind shear or horizontal wind shear.

**1 Introduction**

Eddies play a key role in shaping the mid-latitude atmospheric circulation and climate. They are often generated near the mid-latitude jet stream, where there is strong meridional temperature gradient and strong vertical wind shear, and propagate meridionally outward from the jet in the upper troposphere. By doing so, they converge westerly momentum and thus maintain the jet. At the same time, eddies transport heat poleward and thereby act to reduce the meridional temperature gradient.

Length scale is one of the important aspects of eddies. This is the length scale of the prevalent weather systems we observe in the mid-latitudes. On the one hand, eddy length scale sets the mixing length, which governs the mid-latitude temperature variability (e.g., Schneider et al., 2015). On the other hand, eddy length scale determines eddies' intrinsic zonal phase speed via the Rossby wave's dispersion relationship,  $c - \bar{u} = -\frac{\beta}{k^2 + l^2}$ , where  $c$  is the zonal phase speed,  $\bar{u}$  is the mean zonal wind,  $\beta$  is the gradient of the Coriolis parameter, and  $k$  and  $l$  are the wavenumbers in the zonal and meridional directions. For mean states that are zonally homogeneous and time invariant,  $c$  is conserved. When the waves propagate outward from the jet to latitudes with weaker  $\bar{u}$ ,  $c - \bar{u}$  may no longer be negative and the waves will break at this latitude, referred to as the critical latitude. Therefore, a larger length scale, or a smaller wavenumber, will give a more negative (eastward) relative phase speed and thus may allow the waves to propagate further outward from the jet. Based on how the eddy length scale sets the critical latitude of eddies, stud-

ies (e.g., Kidston et al., 2011) have proposed that increased eddy length scale under global warming can cause a poleward shift of the jet.

Over years, some theories have been proposed to explain the length scale of eddies. In linear baroclinic instability problem of Eady, the most unstable mode has its length scale proportional to the Rossby internal radius of deformation,

$$L_D = \frac{NH}{f}, \quad (1)$$

where  $N$  is the buoyancy frequency,  $H$  is the depth of the fluid, and  $f$  is the Coriolis parameter. In the Charney problem, the  $H$  in this formula is replaced by the depth of the eddies, which is limited by the scale height. In application to the atmosphere,  $H$  in the Rossby radius is often taken as the tropopause height, but sometimes also taken as the pressure scale height (Frierson et al., 2006).

An extension within the linear argument is to consider the nonuniform profile of static stability and vertical wind shear. One can discretize the atmosphere in multiple vertical levels, and numerically solve the quasi-geostrophic (QG) eigenvalue problem to compute the most unstable baroclinic mode and its wavenumber (Smith, 2007; Pfahl et al., 2015; Kang et al., 2019).

Non-linear turbulent theory, on the other hand, suggests that energy will cascade to larger length scale, until it is halted by  $\beta$ . The resulting energy-containing length scale will be proportional to the Rhines scale,

$$L_\beta = \left[ \frac{\text{EKE}^{1/2}}{\beta} \right]^{1/2}, \quad (2)$$

where EKE is the eddy kinetic energy (Rhines, 1975).

The Kuo scale,

$$L_K = \left[ \frac{\bar{u}_{\max}}{\beta} \right]^{1/2}, \quad (3)$$

looks similar, but is dynamically different from the Rhines scale (Vallis, 2006; Nabizadeh et al., 2019). While the Rhines scale inherently comes from non-linear arguments, the Kuo scale can be understood from a linear instability criterion, the Rayleigh-Kuo inflection point criterion, which states that a necessary condition for instability is that  $\beta - \frac{\partial^2}{\partial y^2} \bar{u}$  changes sign (Farrell & Ioannou, 2007; Vallis, 2006). It would therefore set the minimum width of a stable easterly jet. As eddy-eddy interactions can make the flow more isotropic and make the eddy length scale coincide with the jet width (Chemke & Kaspi, 2016), jet width set by the Kuo scale might be linked to the eddy length scale. While the mid-latitudes on the Earth are in a regime of one single westerly jet (rather than alternating easterlies and westerlies), we are including the Kuo scale to be more comprehensive.

The applicability of these length scale arguments, especially of the Rossby radius and the Rhines scale, has been tested in different models and different setups in the past few decades.

In a 2-layer QG model, the Rhines scale is found to match well with the eddy length scale (e.g., Held & Larichev, 1996; Panetta, 1993). In idealized moist general circulation models (GCMs), the Rhines scale is also found to match well with the eddy length scale, when moisture content is varied (Frierson et al., 2006), rotational rate is varied (Chemke & Kaspi, 2016), or when different forcings and boundary conditions are applied (Barry et al., 2002). In between, for an idealized dry GCM, Schneider and Walker (2006) argued that both the Rhines scale and the Rossby radius will fit well with the eddy length scale and it is difficult to separate the two. On the contrary, by varying the thermal expansion coefficient of the fluid in a dry GCM, Jansen and Ferrari (2012) found the Rhines

109 scale and the Rossby radius to be separable and that the Rhines scale fits the eddy length  
110 scale better.

111 Some studies, however, dismissed the applicability of the Rhines scale in describ-  
112 ing the eddy length scale in the atmosphere. In Coupled Model Intercomparison Project,  
113 phase 3 (CMIP3), by doing an inter-model correlation, Kidston et al. (2010) found the  
114 increase of eddy length scale in the 21st century to well correlate with the increase in  
115 static stability ( $N$ ) between 850 and 600 hPa, but they did not find the increase in length  
116 scale to correlate with EKE or magnitude of the poleward shift of jet (surrogate of  $\beta$ ).  
117 In CMIP3, reanalysis and dry GCM, by regressing internal variability on southern an-  
118 nular mode (surrogate of jet shift), Kidston et al. (2011) also found that the shift of jet  
119 and EKE have shortcomings in explaining the variability of length scale, but static sta-  
120 bility ( $N$ ) between 800 and 500 hPa to be consistent with the variations of length scale.  
121 Kidston et al. (2011) also conducted an experiment of increased  $N$  in an idealized dry  
122 GCM, where they found increase in eddy length scale. This experiment was originally  
123 meant to test if increase of length scale can allow waves to propagate further from the  
124 jet and therefore cause the jet to shift poleward. They noted that, unfortunately, the in-  
125 creased  $N$  came with increased meridional temperature gradient, and the influence of  
126  $N$  and meridional temperature gradient became somewhat intractable.

127 With a recent technique of linear response function (LRF, Hassanzadeh & Kuang,  
128 2016), we can now change the static stability without changing meridional temperature  
129 gradient in a dry GCM. While these experiments are idealized and do not closely resem-  
130 ble the global warming, they help with better theoretical understanding of eddies' re-  
131 sponse to the mean state. As we will see in later sections, experiments of increased  $N$   
132 will give us weaker EKE and thus a smaller Rhines scale. We can then test how the Rossby  
133 radius, the Rhines scale, and other length scale arguments work in dry GCM in the con-  
134 text of sole change in static stability.

## 135 2 Methods

### 136 2.1 Dry GCM Ensemble

137 We use the GFDL dry spectral dynamical core with Held and Suarez (1994) forc-  
138 ing. The setup is identical to that of Hassanzadeh and Kuang (2016) with T63 spectral  
139 resolution and 40 vertical levels. Each ensemble consists of 20 runs with slightly differ-  
140 ent initial conditions, and each run is 26,000 days with daily snapshots (first 1,000 days  
141 discarded). The two hemispheres are symmetrically forced, so we present the aggregated  
142 results. Each ensemble will then have 1,000,000 days of valid data. Such large ensem-  
143 ble size and long simulation allow us to have small uncertainty in the meridional tem-  
144 perature gradient.

### 145 2.2 Forced Experiments

146 The following ensemble experiments are conducted in comparison to the above con-  
147 trol ensemble experiment:

148 **K11:** This experiment applies the forcing in the  $N_{\text{increased}}$  experiment in Kidston  
149 et al. (2011). The equilibrium temperature ( $T_{\text{eq}}$ ) field in the Newtonian relaxation is de-  
150 creased by 3 K at  $\sigma > 0.85$ , where  $\sigma$  is pressure divided by surface pressure. Chang-  
151 ing  $T_{\text{eq}}$  is equivalent to a temperature forcing in  $\text{K day}^{-1}$ , as converted by the Newto-  
152 nian relaxation rate.

153 **LRF:** This experiment uses a time-invariant and zonally-uniform forcing (see sub-  
154 section 2.3) to force the atmosphere towards a target mean state change. The temper-  
155 ature part of this target change is set to the meridional average of the temperature change

156 in experiment K11 (around 2 K decrease near surface). The zonal wind part of this tar-  
 157 get change is set to zero.

158 K11–LRF: This experiment is K11 minus LRF, which applies the forcing in K11  
 159 plus the opposite forcing in experiment LRF. If the mean state change is linear to the  
 160 forcing applied, the meridional temperature gradient will change without changing the  
 161 mean static stability.

162 0.5×LRF, -0.5×LRF, -1.0×LRF: These are 3 more experiments with 0.5, -0.5, and  
 163 -1.0 times the forcing in experiment LRF.

### 164 2.3 Iterative Use of Linear Response Function

165 The above-mentioned experiment LRF needs to find a time-invariant and zonally-  
 166 uniform forcing to force a target mean state change. Being time-invariant and zonally  
 167 uniform, the forcing does not directly act on the eddies. Some previous approaches (e.g.,  
 168 Yuval & Kaspi, 2020) do not have this merit. We find the forcing by iterative use of a  
 169 LRF matrix as follows. We have a LRF matrix  $\mathbf{L}$  of this dry GCM constructed in Hassanzadeh  
 170 and Kuang (2016). For a state vector  $\bar{\mathbf{x}}$  consisting of zonal mean temperature and zonal  
 171 wind,  $\mathbf{L}$  is a square matrix that linearly relates the target mean state change  $\bar{\mathbf{x}}_{\text{target}}$  and  
 172 the required forcing  $\bar{\mathbf{f}}_1$ , as  $\bar{\mathbf{f}}_1 = -\mathbf{L}\bar{\mathbf{x}}_{\text{target}}$ . The first iteration uses forcing  $\bar{\mathbf{f}}_1$  and pro-  
 173 duces a mean state change  $\bar{\mathbf{x}}_1$ . Because the LRF matrix is not perfect,  $\bar{\mathbf{x}}_1$  may not be  
 174 as close to  $\bar{\mathbf{x}}_{\text{target}}$  as needed. The  $n$ -th iteration takes forcing  $\bar{\mathbf{f}}_n = \bar{\mathbf{f}}_{n-1} - \mathbf{L}(\bar{\mathbf{x}}_{\text{target}} - \bar{\mathbf{x}}_{n-1})$   
 175 and produces a mean state change  $\bar{\mathbf{x}}_n$ . In our case, the second iteration gives a satisfac-  
 176 tory mean state as shown later.

### 177 2.4 Mean State

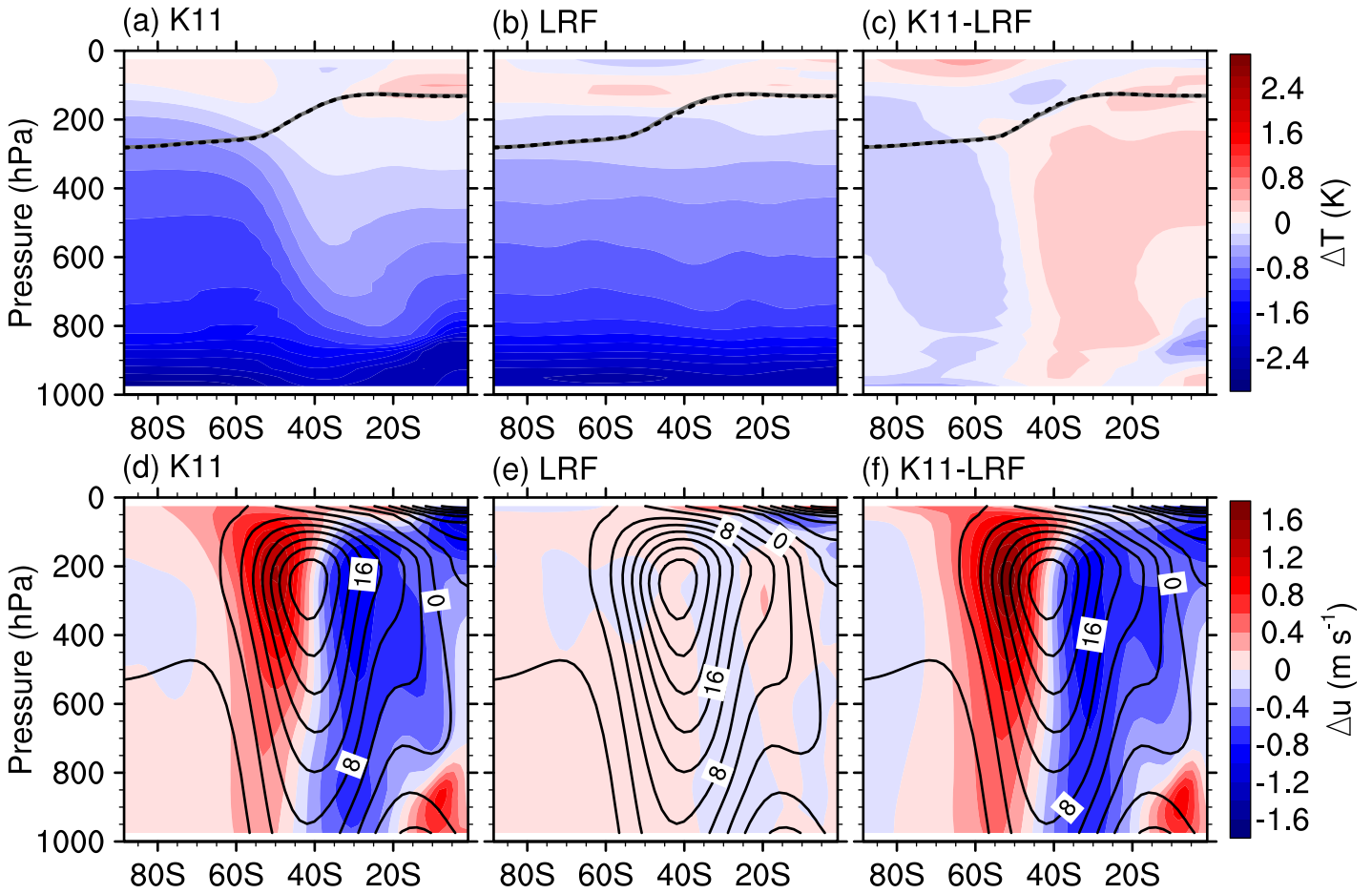
183 Our K11 experiment reproduces the mean state change in the  $N_{\text{increased}}$  experiment  
 184 in Kidston et al. (2011) reasonably well (Figure 1). The experiment comes with a no-  
 185 ticeably increased meridional temperature gradient around 50S. According to the ther-  
 186 mal wind balance, such change in meridional temperature gradient will give rise to change  
 187 in zonal wind. Hereafter, we quantify the change in zonal wind as an indirect measure  
 188 of meridional temperature gradient. The change of zonal wind reaches around  $1.4 \text{ m s}^{-1}$   
 189 in experiment K11. Such changes in meridional temperature gradient and zonal wind  
 190 make it hard to attribute the eddies response solely to the increased  $N$ .

191 Our LRF experiment targets a mean state with increased  $N$  without changing merid-  
 192 ional temperature gradient. The experiment successfully produces much weaker change  
 193 in meridional temperature gradient, and change in zonal wind is mostly smaller than  $0.2 \text{ m s}^{-1}$   
 194 except near the model top (Figure 1). We note that with our 1,000,000-day-equivalent  
 195 ensembles, the 95% confidence interval of the difference between two ensembles is smaller  
 196 than  $0.14 \text{ m s}^{-1}$  for zonal wind (not shown). This very narrow confidence interval is help-  
 197 ful to the success of getting a small change in meridional temperature gradient, especially  
 198 when we are using an iterative approach.

199 Experiment K11–LRF has its mean state change roughly equal to the difference  
 200 between K11 and LRF, which changes meridional temperature gradient without chang-  
 201 ing the mean static stability (Figure 1). This indicates that the mean state is reason-  
 202 ably linear to the forcing.

### 203 2.5 Spectral Decomposition

204 We decompose zonal and meridional winds  $u$  and  $v$  into zonal spectra  $\tilde{U}_k$  and  $\tilde{V}_k$ .  
 205 At zonal wavenumber  $k$ ,  $\overline{v'^2}$  will then be  $0.5 \times \left| \tilde{V}_k \right|^2$ , and  $\overline{u'^2}$  will be  $0.5 \times \left| \tilde{U}_k \right|^2$ .



178 **Figure 1.** Mean temperature change (top) and zonal wind change (bottom) in experiments  
 179 K11 (left), LRF (middle), and K11–LRF (right). Lines in the top panels show the World Meteorological Organization (WMO) tropopause in the control experiment (gray solid) and the forced  
 180 experiments (black dotted). Contours in the bottom panels show the climatological zonal wind in  
 181 the control experiment.  
 182

206 Following Chemke and Kaspi (2016), we define energy-containing zonal wavenum-  
 207 ber  $k_e$  (at each latitude  $\phi$ ) as the “squared inverse centroid” of the zonal spectrum of  
 208 barotropic  $\overline{v'^2}$  as follows:

$$209 \quad k_e^{-2} = \frac{\sum_k k^{-2} |\tilde{V}_k|^2}{\sum_k |\tilde{V}_k|^2} \quad (4)$$

210 and the energy-containing zonal scale  $L_e$  is  $2\pi a \cos \phi / k_e$ , where  $a$  is the Earth's radius.

211 To decompose momentum flux in zonal phase speeds (Randel & Held, 1991), we  
 212 first decompose  $u$  and  $v$  at every 100-day slot into zonal wavenumber–frequency spec-  
 213 tra  $\tilde{U}_{k,\omega}$  and  $\tilde{V}_{k,\omega}$ . At zonal wavenumber  $k$  and frequency  $\omega$ ,  $\overline{u'v'}$  will be  $0.5 \times \text{Re} \left[ \tilde{U}_{k,\omega} \tilde{V}_{k,\omega}^* \right]$ ,  
 214 where asterisk \* denotes the complex conjugate. Then,  $\overline{u'v'}$  is averaged across differ-  
 215 ent 100-day slots and different ensemble members. Next, notice that angular phase speed  
 216  $c / \cos \phi = \omega a / k$ . We use a  $1 \text{ m s}^{-1}$  bin size in angular phase speed and sum up the pro-  
 217 portionate spectrum according to the fraction of  $(k, \omega)$  grid giving  $c - 0.5 \leq \omega a / k < c + 0.5$ .

218 The momentum flux convergence is calculated as equation 9 in Kidston et al. (2011)

$$219 \quad -\frac{1}{a \cos^2 \phi} \frac{\partial}{\partial \phi} \overline{u'v'} \cos^2 \phi. \quad (5)$$

220 The latitude partial derivative is done in constant *absolute* angular phase speed. After-  
 221 wards, this flux convergence is plotted in relative angular phase speed  $(c - \bar{u}) / \cos \phi$ .

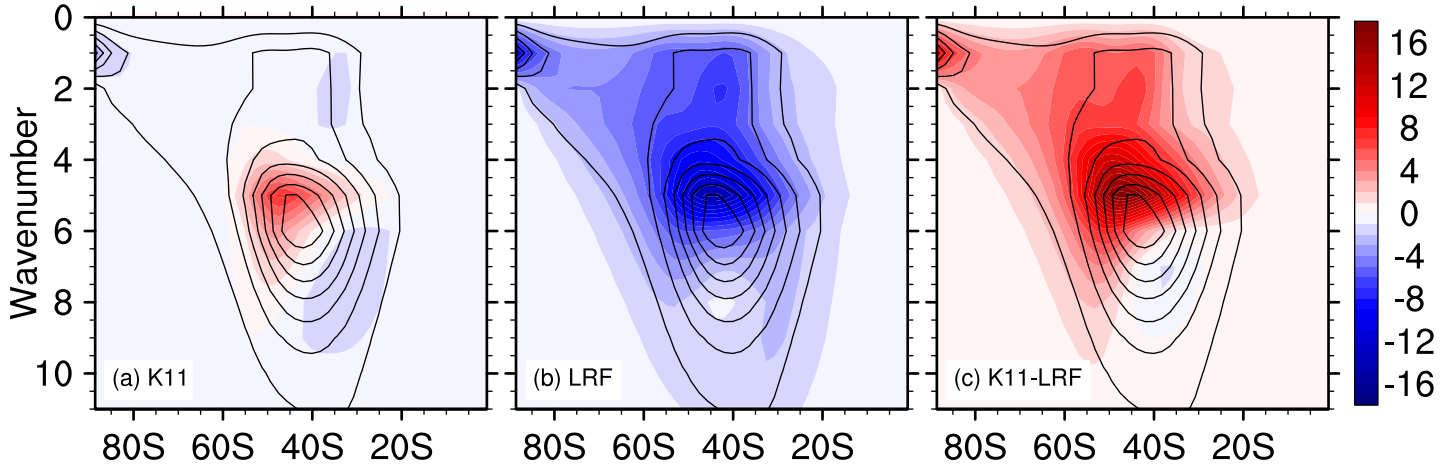
## 222 2.6 Linear Baroclinic Instability Calculation

223 We use the linear baroclinic instability calculation code that is described on page 9381  
 224 of Pfahl et al. (2015). Briefly, it solves the linearized QG potential vorticity equation in  
 225 pressure coordinate as an eigenvalue problem. The code inputs vertical profiles of zonal  
 226 wind and thermal stratification from the mean state of the GCM. For boundary condi-  
 227 tions, the vertical velocity in pressure coordinate is zero at the model top (0 hPa) and  
 228 the vertical velocity in height coordinate is set to zero at the surface. We adapt the Rayleigh  
 229 damping of low-level winds in the code to be the same rate as the GCM, with maximum  
 230 drag coefficient of  $1 \text{ day}^{-1}$  (Held & Suarez, 1994). Newtonian relaxation of temperature  
 231 is not applied. The meridional wavenumber is set to zero. For each  $k$ , the code calcu-  
 232 lates a vector of complex eigenvalues (the real part is the growth rate and the imaginary  
 233 part is the frequency) and outputs the complex eigenvalue with the largest positive real  
 234 part. The  $k$  outputting eigenvalue with the largest positive real part will give us the max-  
 235 imum baroclinic growth scale,  $L_{\text{grow}}$ .

## 236 2.7 Rossby Radius and Rhines Scale

237 The Rossby radius is calculated as equation (1), where the tropopause height  $H$   
 238 is calculated based on the WMO definition, and similar to Chemke and Kaspi (2016) and  
 239 Frierson et al. (2006), the static stability  $N$  is calculated as  $N = \sqrt{\frac{g (\ln \theta_{\text{trop}} - \ln \theta_{\text{bot}})}{H}}$   
 240 with  $\theta_{\text{trop}}$  being the potential temperature at the tropopause and  $\theta_{\text{bot}}$  being the poten-  
 241 tial temperature at the lowest level.

242 The Rhines scale is calculated as equation (2), where EKE is calculated as the ver-  
 243 tically averaged  $\frac{1}{2} (\overline{u'^2} + \overline{v'^2})$  (similar to Chemke & Kaspi, 2016).



246 **Figure 2.** Zonal spectra of  $\frac{1}{2} (\overline{u'^2} + \overline{v'^2})$  at 300 hPa ( $\text{m}^2\text{s}^{-2}$ ) in experiments K11 (a),  
 247 LRF (b), and K11-LRF (c). Black contours show the spectra in the control experiment at  
 248 intervals of 10.

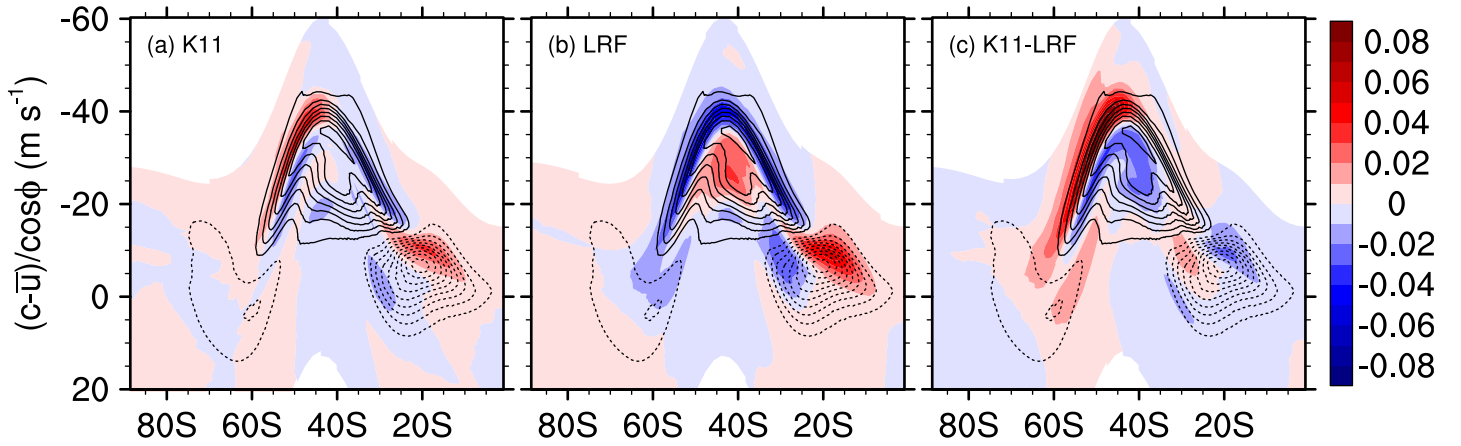
### 244 3 Results

#### 245 3.1 Eddy Spectra

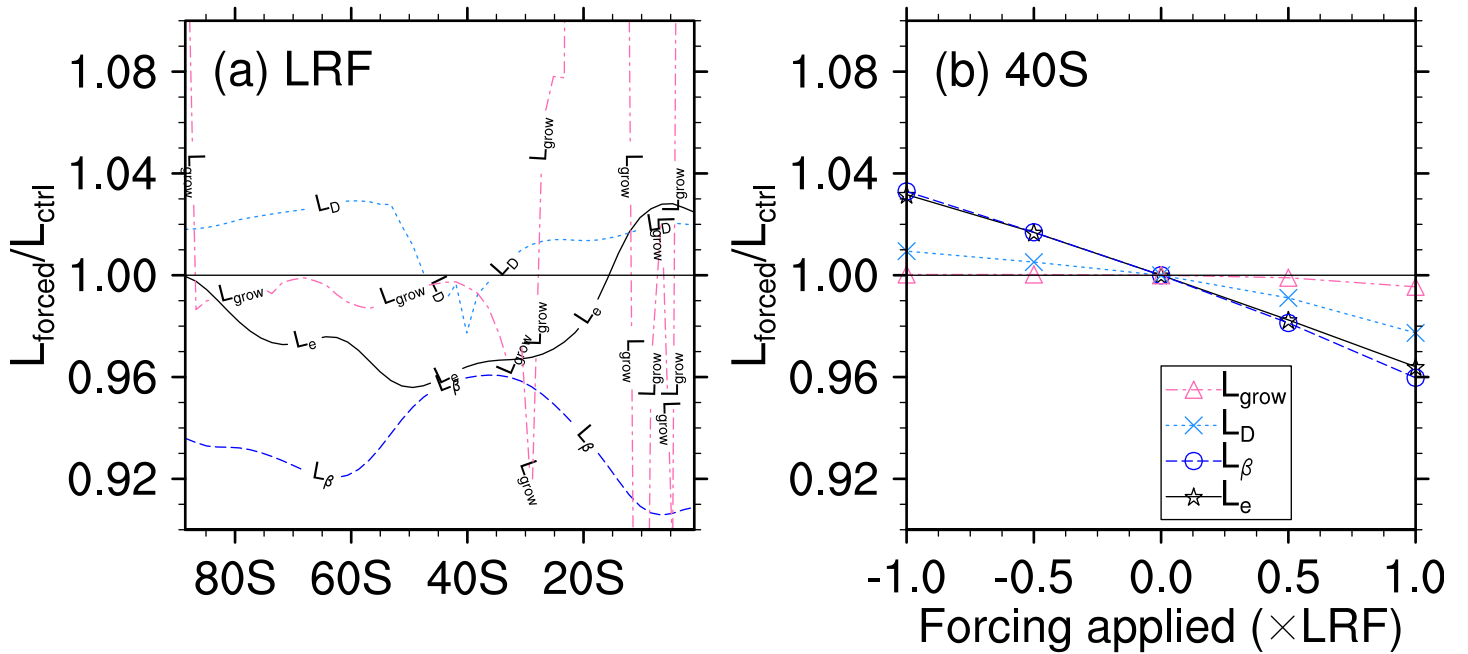
249 In experiment K11, we qualitatively reproduce results in Kidston et al. (2011) that  
 250 the zonal scale of eddies increases, and eddies shift poleward (Figure 2a).

251 In our LRF experiment, we find EKE decreases at every zonal wavenumber and  
 252 latitude (Figure 2b). Stronger decrease happens at smaller zonal wavenumbers, causing  
 253 a decreased eddy zonal scale. This decreasing zonal scale is opposite to that of exper-  
 254 iment K11, which suggests that the change in meridional temperature gradient is impor-  
 255 tant in controlling the eddy length scale and played a role in the conclusion of Kidston  
 256 et al. (2011). It is clearer in experiment K11-LRF, which only increases meridional tem-  
 257 perature gradient without changing the mean static stability. The increase in meridional  
 258 temperature gradient causes a strong increase of EKE at small zonal wavenumbers. It  
 259 dominates over the effect of increased static stability and causes the eddy zonal scale to  
 260 increase in experiment K11. Here the EKE response in K11 is roughly the sum of those  
 261 in LRF and K11-LRF, suggesting that this is roughly linear to the forcing added.

266 In their study of the jet's poleward shift under climate change, Kidston et al. (2011)  
 267 proposed that an increase of static stability will increase the eddy length scale, which  
 268 will make the relative phase speed of eddies more negative, i.e., westward. In this line  
 269 of thought, Figure 3 is more relevant, which plots momentum flux convergence as a func-  
 270 tion of relative angular phase speed and latitude, following Figure 6 in Kidston et al. (2011).  
 271 In experiment K11, like zonal spectrum of EKE (Figure 2a), momentum flux convergence  
 272 shifts poleward and to more negative relative phase speed (Figure 3a). In experiment  
 273 LRF, in contrast, momentum flux convergence does not shift meridionally but shifts to  
 274 less negative phase speed (Figure 3b). So increased wavenumber of EKE in Figure 2b  
 275 does correspond to less negative phase speed of momentum flux convergence. In exper-  
 276 iment K11-LRF, there is a stronger shift, poleward and towards more negative (west-  
 277 ward) relative phase speed (Figure 3c).



262 **Figure 3.** Momentum flux convergence at 300 hPa ( $\text{m s}^{-1}\text{day}^{-1}$  per  $\text{m s}^{-1}$  bin), as a  
 263 function of relative angular phase speed and latitude, in experiments K11 (a), LRF (b), and  
 264 K11-LRF (c). Black contours show the momentum flux convergence (solid) and divergence (dot-  
 265 ted) in the control experiment at intervals of 0.025.



279 **Figure 4.** Length scales in forced experiments divided by those in the control experiment: at  
 280 different latitudes in experiment LRF (a) and at  $40^\circ\text{S}$  in different experiments (b). Shown are the  
 281 energy-containing zonal scale  $L_e$ , the Rhines scale  $L_\beta$ , the Rossby radius  $L_D$  and the maximum  
 282 baroclinic growth scale  $L_{\text{grow}}$ . The Kuo scale  $L_K$  is not shown and is unchanged. The maximum  
 283 baroclinic growth scale  $L_{\text{grow}}$  is not accurate equatorward of  $30^\circ\text{S}$ .

### 3.2 Evaluating Eddy Length Scale Theories

Now, let us compare different length scale arguments in experiment LRF. The actual energy-containing zonal scale decreases by around 3 to 4% (Figure 4a), which matches with Rhines scale near the jet core. When forcing is applied in different signs and magnitudes, similar behaviors are found (Figure 4b). Therefore, the results here are robust. The Rossby radius generally increases by around 2%, which is opposite to the observed decrease of the energy-containing zonal scale,  $L_e$  (Figure 4a).

The maximum baroclinic growth scale decreases by around 1%, which is less than the observed decrease of  $L_e$ . By accounting for the non-uniform profile of static stability and zonal wind, this scale goes in the opposite direction to static stability or the Rossby radius. The difference between this scale and the Rossby radius is also noted by Chemke and Kaspi (2016). Note that even more ideally, the maximum baroclinic growth scale should be calculated globally accounting for meridional variations, rather than locally at each latitude.

The Rhines scale decreases by around 4 to 8%. It matches well with the observed change of  $L_e$  near the jet core. Away from the jet (or latitude of maximum EKE), the Rhines scale decreases more than the observed eddy length scale. This is somewhat consistent with Frierson et al. (2006), who found the Rhines scale at the latitude of maximum EKE to work better than the local Rhines scale. The latter was too sensitive to moisture content in their moist GCM. Also, note that the Rhines scale changes in the opposite direction as the Rossby radius does, and this is in contrast to the findings of Schneider and Walker (2006), who suggested that the Rhines scale and the Rossby radius change in the same way and cannot be separated.

The Kuo scale remains basically unchanged (not shown), as the mean zonal wind in this experiment remains basically unchanged. The Kuo scale does not agree with the observed change in  $L_e$ .

## 4 Conclusions and Discussions

With iterative use of the LRF of an idealized dry GCM, we are able to increase the static stability with very small change in the meridional temperature gradient and zonal wind, by a time-invariant and zonally-uniform forcing. The change in meridional temperature gradient, as measured by change in zonal wind, is mostly less than  $0.2 \text{ m s}^{-1}$  when temperature near surface is cooled by more than 2 K. In this well-controlled experiment, the energy-containing zonal scale decreases with increased static stability. We also find momentum flux convergence to shift towards less negative relative phase speed, consistent with a decreased length scale. This is against the argument of Kidston et al. (2011) and the Rossby radius as eddy length scale, which would predict length scale to increase with static stability.

In this well-controlled experiment, we also quantitatively tested the applicability of several length scale arguments. In experiment LRF (around 2 K decrease near surface), we find energy-containing zonal scale to decrease by around 3 to 4%, which matches well with the Rhines scale near the jet core. Rossby radius (+2%), the maximum baroclinic growth scale (-1%) and the Kuo scale (0%) do not match the observed change in eddy length scale. Additional controlled experiments in which the sign and/or magnitude of the forcing are changed further confirm that the zonal eddy length scale varies linearly with the Rhines scale (Figure 4b).

Here our focus is the statistics of equilibrated eddies. Non-equilibrated eddies may not respond to static stability in the same way we see here. Therefore, our results may not apply to internal variability of eddy length scale, which is also analyzed by Kidston et al. (2011).

Our well-controlled experiment of increased static stability without changing the mean zonal wind may also be used to analyze other statistics of equilibrated eddies, for example, on how they transport momentum and heat. One might notice that in experiment LRF, EKE decreases at all zonal wavenumbers (Figure 2b), while momentum flux convergence locally strengthened at some relative phase speeds and latitudes (Figure 3b). This could suggest a more efficient momentum transport per EKE in this experiment and is being studied in future work.

Our framework of forcing a mean state can further be applied to more realistic models such as an idealized moist GCM, in which we can see the effect of moisture.

## Acknowledgments

This paper is substantially based on the first author’s PhD dissertation (Chan, 2020). The computations in this paper were run on the FASRC Cannon cluster supported by the FAS Division of Science Research Computing Group at Harvard University. The authors thank Paul O’Gorman, Ebrahim Nabizadeh, Brian Farrell, Peter Huybers, Eli Tziperman, Wanying Kang, Duo Chan and Lei Wang for fruitful discussions. P. W. C. and Z. K. are supported by NSF grant AGS1552385, NASA grant 80NSSC17K0267 and a grant from the Harvard Global Institute. P. H. is supported by NSF grant AGS-1921413.

## Data Availability Statement

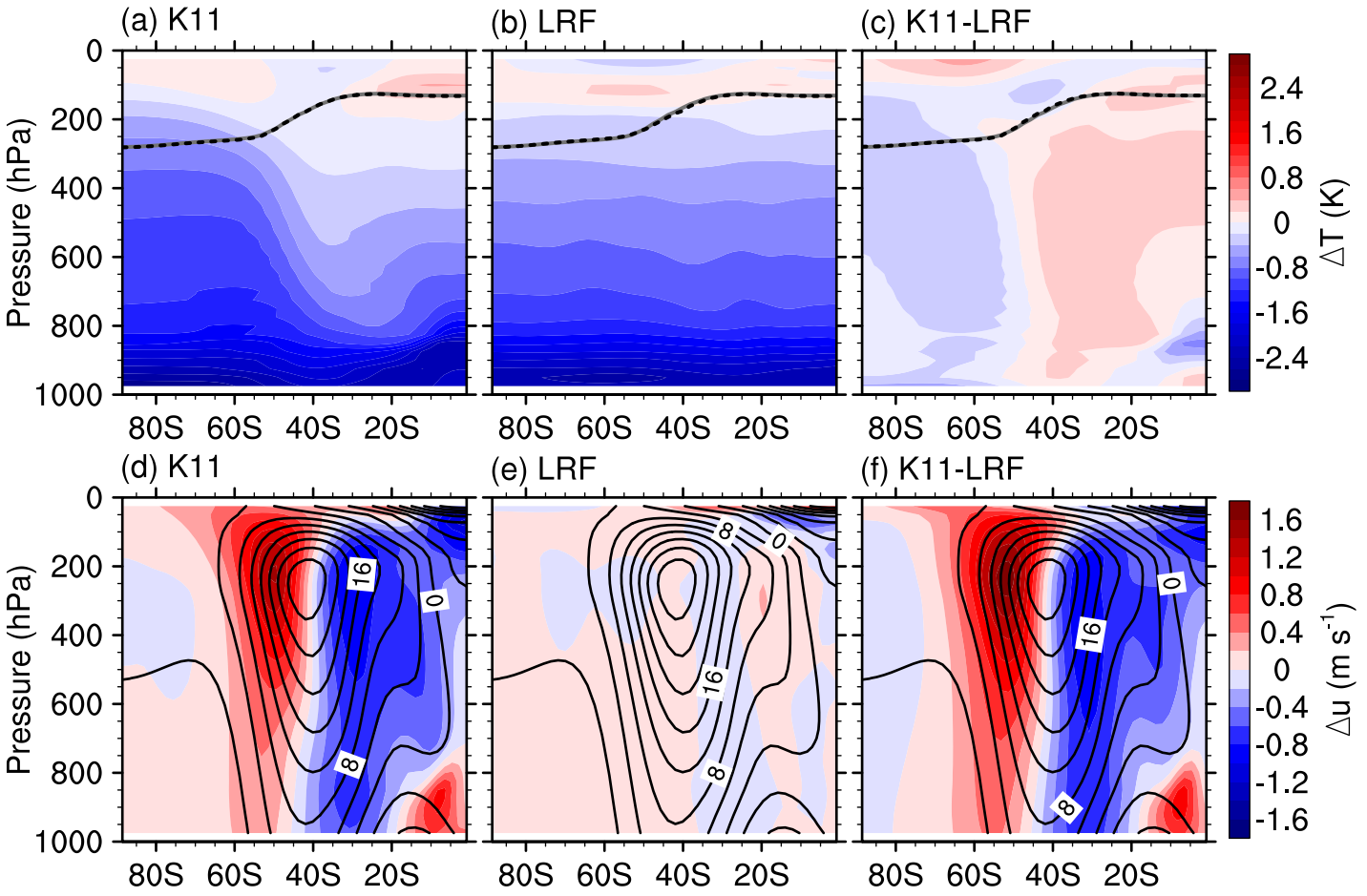
The linear baroclinic instability code is provided by Paul O’Gorman. The GFDL dry spectral dynamical core can be acquired from <https://www.gfdl.noaa.gov/idealized-spectral-models-quickstart/>. “The NCAR Command Language (Version 6.6.2)” (2019) is obtained from <https://doi.org/10.5065/D6WD3XH5>. Data displayed in this paper are available from <https://github.com/PackardChan/chk2021-lengthscale-dry>.

## References

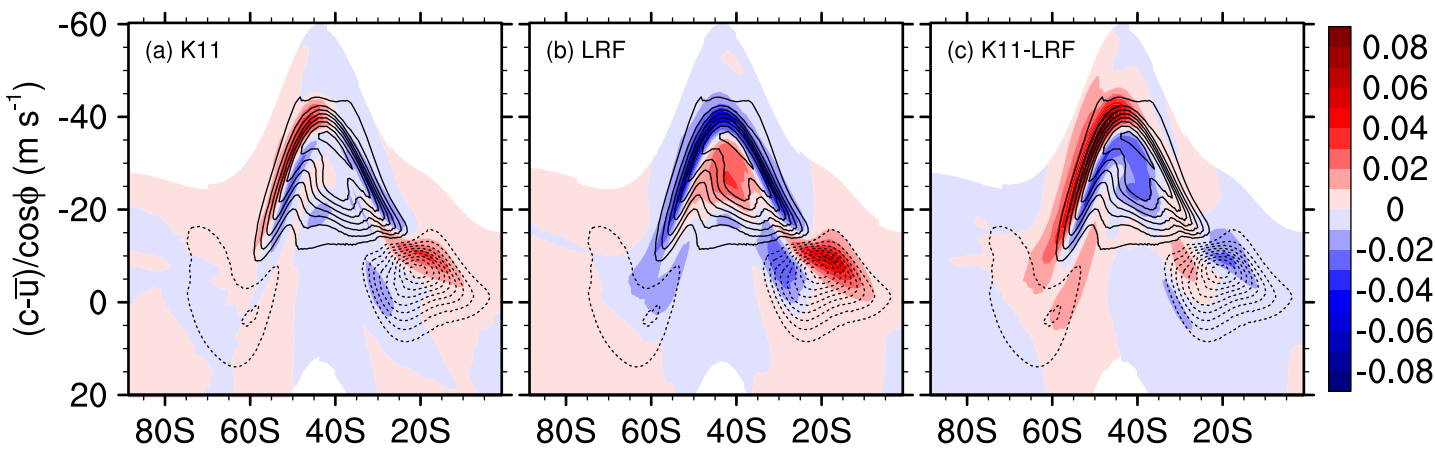
- Barry, L., Craig, G. C., & Thuburn, J. (2002). Poleward heat transport by the atmospheric heat engine [Journal Article]. *Nature*, *415*(6873), 774-777. doi: 10.1038/415774a
- Chan, P. W. (2020). *Evaluating blocking indices and investigating eddies response to static stability* (Doctoral dissertation, Harvard University). Retrieved from <https://search.proquest.com/docview/2467866555>
- Chemke, R., & Kaspi, Y. (2016). The effect of eddy–eddy interactions on jet formation and macroturbulent scales [Journal Article]. *Journal of the Atmospheric Sciences*, *73*(5), 2049-2059. doi: 10.1175/Jas-D-15-0375.1
- Farrell, B. F., & Ioannou, P. J. (2007). Structure and spacing of jets in barotropic turbulence [Journal Article]. *Journal of the Atmospheric Sciences*, *64*(10), 3652-3665. doi: 10.1175/JAS4016.1
- Frierson, D. M. W., Held, I. M., & Zurita-Gotor, P. (2006). A gray-radiation aquaplanet moist GCM. Part I: Static stability and eddy scale [Journal Article]. *Journal of the Atmospheric Sciences*, *63*(10), 2548-2566. doi: 10.1175/Jas3753.1
- Hassanzadeh, P., & Kuang, Z. (2016). The linear response function of an idealized atmosphere. Part I: Construction using Green’s functions and applications [Journal Article]. *Journal of the Atmospheric Sciences*, *73*(9), 3423-3439. doi: 10.1175/JAS-D-15-0338.1
- Held, I. M., & Larichev, V. D. (1996). A scaling theory for horizontally homogeneous, baroclinically unstable flow on a beta plane [Journal Article]. *Journal of the Atmospheric Sciences*, *53*(7), 946-952. doi: 10.1175/1520-0469(1996)053<0946:Astfhh>2.0.Co;2
- Held, I. M., & Suarez, M. J. (1994). A proposal for the intercomparison of the dy-

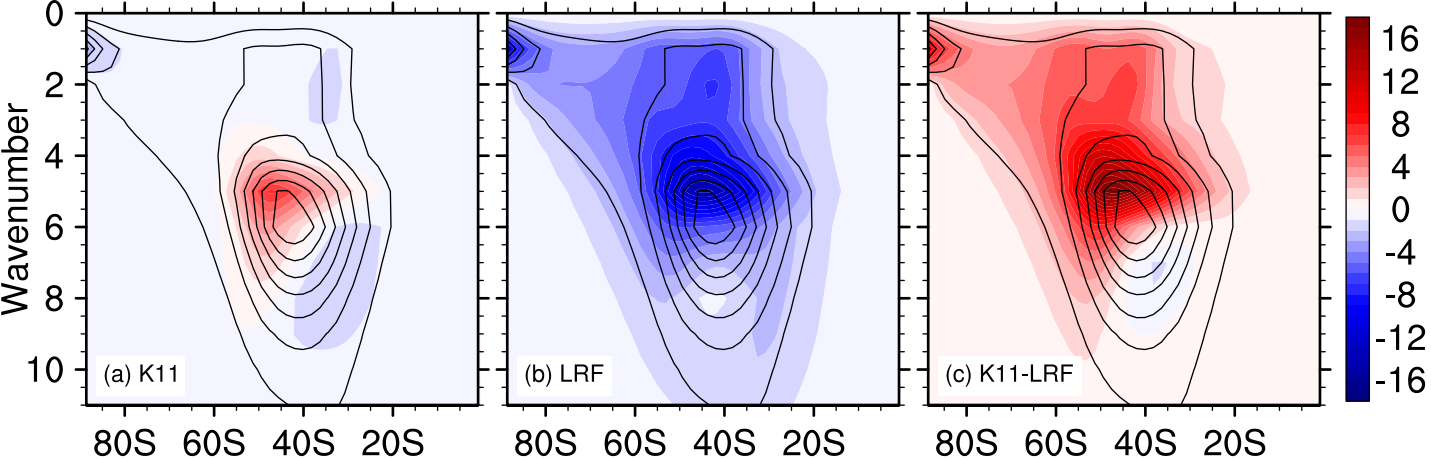
- 381 namical cores of atmospheric general circulation Models [Journal Article]. *Bul-*  
 382 *letin of the American Meteorological Society*, 75(10), 1825-1830. doi: 10.1175/  
 383 1520-0477(1994)075(1825:Apftio)2.0.Co;2
- 384 Jansen, M., & Ferrari, R. (2012). Macroturbulent equilibration in a thermally forced  
 385 primitive equation system [Journal Article]. *Journal of the Atmospheric Sci-*  
 386 *ences*, 69(2), 695-713. doi: 10.1175/Jas-D-11-041.1
- 387 Kang, W., Cai, M., & Tziperman, E. (2019). Tropical and extratropical general  
 388 circulation with a meridional reversed temperature gradient as expected  
 389 in a high obliquity planet [Journal Article]. *Icarus*, 330, 142-154. doi:  
 390 10.1016/j.icarus.2019.04.028
- 391 Kidston, J., Dean, S. M., Renwick, J. A., & Vallis, G. K. (2010). A robust increase  
 392 in the eddy length scale in the simulation of future climates [Journal Article].  
 393 *Geophysical Research Letters*, 37(3), L03806. doi: 10.1029/2009gl041615
- 394 Kidston, J., Vallis, G. K., Dean, S. M., & Renwick, J. A. (2011). Can the increase  
 395 in the eddy length scale under global warming cause the poleward shift of the  
 396 jet streams? [Journal Article]. *Journal of Climate*, 24(14), 3764-3780. doi:  
 397 10.1175/2010JCLI3738.1
- 398 Nabizadeh, E., Hassanzadeh, P., Yang, D., & Barnes, E. A. (2019). Size of the  
 399 atmospheric blocking events: Scaling law and response to climate change  
 400 [Journal Article]. *Geophysical Research Letters*, 46(22), 13488-13499. doi:  
 401 10.1029/2019GL084863
- 402 The NCAR Command Language (Version 6.6.2) [Computer software]. (2019). Boul-  
 403 der, Colorado: UCAR/NCAR/CISL/TDD. doi: 10.5065/D6WD3XH5
- 404 Panetta, R. L. (1993). Zonal jets in wide baroclinically unstable regions: Persistence  
 405 and scale selection [Journal Article]. *Journal of the Atmospheric Sciences*,  
 406 50(14), 2073-2106. doi: 10.1175/1520-0469(1993)050(2073:ZJIWBU)2.0.CO;2
- 407 Pfahl, S., OGorman, P. A., & Singh, M. S. (2015). Extratropical cyclones in ide-  
 408 alized simulations of changed climates [Journal Article]. *Journal of Climate*,  
 409 28(23), 9373-9392. doi: 10.1175/Jcli-D-14-00816.1
- 410 Randel, W. J., & Held, I. M. (1991). Phase speed spectra of transient eddy fluxes  
 411 and critical layer absorption [Journal Article]. *Journal of the Atmospheric Sci-*  
 412 *ences*, 48(5), 688-697. doi: 10.1175/1520-0469(1991)048(0688:PSSOTE)2.0.CO;  
 413 2
- 414 Rhines, P. B. (1975). Waves and turbulence on a beta-plane [Journal Article]. *Jour-*  
 415 *nal of Fluid Mechanics*, 69(03), 417-443. doi: 10.1017/S0022112075001504
- 416 Schneider, T., Bischoff, T., & Płotka, H. (2015). Physics of changes in synoptic mid-  
 417 latitude temperature variability [Journal Article]. *Journal of Climate*, 28(6),  
 418 2312-2331. doi: 10.1175/JCLI-D-14-00632.1
- 419 Schneider, T., & Walker, C. C. (2006). Self-organization of atmospheric macrotur-  
 420 bulance into critical states of weak nonlinear eddy-eddy interactions [Jour-  
 421 nal Article]. *Journal of the Atmospheric Sciences*, 63(6), 1569-1586. doi:  
 422 10.1175/Jas3699.1
- 423 Smith, K. S. (2007). The geography of linear baroclinic instability in Earth's oceans  
 424 [Journal Article]. *Journal of Marine Research*, 65(5), 655-683. doi: 10.1357/  
 425 002224007783649484
- 426 Vallis, G. K. (2006). *Atmospheric and Oceanic Fluid Dynamics: Fundamentals and*  
 427 *Large-Scale Circulation* [Book]. Cambridge University Press.
- 428 Yuval, J., & Kaspi, Y. (2020). Eddy activity response to global warminglike temper-  
 429 ature changes [Journal Article]. *Journal of Climate*, 33(4), 1381-1404. doi: 10  
 430 .1175/JCLI-D-19-0190.1

Figure 1.



Figures 3 and 2.





**Figure 4.**

